# Adaptive hybrid particle swarm optimization and fuzzy logic controller for a solar-wind hybrid power system

**G. B. Arjun Kumar[1], M. Balamurugan[1], K. N. Sunil Kumar[2], Ravi Gatti[3]**

[1]Department of Electrical and Electronics Engineering, Dayananda Sagar College of Engineering,
Visvesvaraya Technological University, Bengaluru, India
[2]Department of Information Science and Engineering, Sri Venkateshwara College of Engineering,
Visvesvaraya Technological University, Bengaluru, India
[3]Department of Electronics and Communication Engineering, Dayananda Sagar Academy of Technology and Management,
Bengaluru, India

| Article Info | ABSTRACT |
|---|---|
| | This paper presents the best modeling and control strategies for a grid-connected hybrid wind-solar power system to maximize energy production. For variable wind speeds, determine the optimal power point using fuzzy logic control, adopt an adaptive hill climb searching method, and compare it with an optimal torque control method for large inertia wind turbine (WT). The role of fuzzy logic controller (FLC) is to adjust the hill climbing search (HCS) technique's step-size according to the operating point. The doubly-fed induction generator (DFIG) control system has two subsystems: rotor-side and grid-side converters. The active and reactive power have been indirectly regulated by adjusting the current on the d-q axis. The rotor side converter (RSC) controllers are responsible for controlling the WTs rotational speed to achieve the maximum power output. The grid side converter (GSC) manages the voltage at the DC link and keeps a unity power factor between the grid and GSC. Optimal hybrid power point tracking technique for use with photovoltaic systems in both constant and variable shade circumstances, based on particle swarm optimization (PSO) and perturb and observe (P&O). The optimal power point tracking (OPPT) approach is compared to three other methods: PSO, P&O, and hybrid P&O-PSO. The model has a total capacity of 2.249 MW, with wind capacity of 2 MW and solar capacity of 0.249 MW, and its efficiency is analyzed. |

*Corresponding Author:*

G. B. Arjun Kumar
Department of Electrical and Electronics Engineering, Dayananda Sagar College of Engineering
Visvesvaraya Technological University
Bengaluru, Karnataka 560078, India
Email: arjun-eee@dayanandasagar.edu

## 1. INTRODUCTION

Since the world's energy needs are growing, more renewable energy sources (RESs) are being used. This is to avoid the problems that come with fossil fuels, such as their high cost, quick depletion, and environment pollution. Nowadays, RESs have been deployed extensively due to their environmental friendliness and accessibility. Researchers anticipate producing pollution-free electricity with the use of RESs. Biomass, the sun, wind, and water are examples of naturally occurring, non-exhaustible, and non-polluting renewable sources of energy [1].

Optimization techniques for the design of a solar-wind hybrid power system (SWHPS) ensure electricity reliability while reducing system costs. SWHPS ensures a constant supply of electricity to end

consumers [2]. A hybrid system employs multiple energy sources, such as wind and solar photovoltaic (SPV), and is available with or without backup batteries [3]. The objective is to place greater emphasis on harnessing green energy resources in order to gradually decommission the traditional electrical grid, thereby reducing electric power bills.

Wind energy is anticipated to meet 20% of the world's energy needs by 2030 and is considered to be a viable source of energy. The collective wind power capacity reached 744 GW in 2020, covering more than 5% of worldwide electricity consumption [4]. The worldwide wind capacity reached 955 GW by the end of 2022. India's ability to make wind power has grown a lot in the last few years. As of January 31, 2023, the cumulative installed capacity of wind power was 42 GW, which made it the 4th largest installed capacity of wind power in the world [5].

The wind energy conversion system (WECS) has been enhanced over the past several decades to accommodate the rapid development of industrial wind technology. The wind turbine (WT) is the most important part of the WECS because it turns the kinetic energy of the wind into mechanical energy. On the global market, there are two different ways to set up WT. Compared to the variable speed wind turbine (VSWT), the fixed speed wind turbine (FSWT) is easy to build and has a small range of wind speeds. The VSWT has a number of advantages, including a high wind energy collection rate and a broad speed range with total controllability. Several generator types, including squirrel-cage induction generators (SCIGs), doubly-fed induction generators (DFIGs), and permanent magnet synchronous generators (PMSGs), are utilized in variable-speed WECS [6].

Doubly fed induction generators (DFIGs) have gained significant popularity in the context of large-scale WECS. Consequently, extensive research has been conducted in recent years to investigate their operational and control aspects [7]. The operation of wind turbines is restricted to a predetermined range of wind velocities, which are delimited by cut-in and cut-out speeds. The WT must be halted beyond these boundaries to safeguard both the turbine and generator [8].

An optimum power point tracking (OPPT) algorithm must be incorporated into the system in order to determine the optimum working point of the WT. Many articles have been written about OPPT algorithms, such as power signal feedback (PSF) control, tip speed ratio (TSR) control, robust control, hill-climb searching (HCS) control, and optimal torque (OT) control [9], [10]. TSR control modulates the WT rotor speed to maintain an optimal TSR at which optimum power is extracted; nevertheless, this method has limitations due to the challenge of obtaining the optimum TSR and accurately measuring wind speed [11]. PSF and OT techniques need to know the optimum power curve (OPC) of the wind turbine. The control methods of the WT follows this curve. According to [12], it's hard to implement the model predictive control (MPC) accurately in practical implementations. The HCS method doesn't need data on wind speed or information on the turbine's attributes.

Numerous techniques have been investigated in the literature to enhance the HCS [13]. The adjustment mechanism for regulating the step size differs across various research groups, depending on the perturbed variable [14]. A few researchers used the converter's duty cycle as a control input to the system [15]. In some cases, the input voltage or the load current are applied as control inputs [16]. The research utilized the variation between the present speed of the generator ($\omega$) and its optimum speed ($\omega^*$) ascertained from the optimal power curve to systematically adjust the magnitude of perturbation at the completion of each cycle [17]. Studied many written wind OPPT approaches and decided that these two are the best because they can adapt to changing conditions and tune themselves [18].

The photovoltaic (PV) solar power generation is a technology that has been expanding rapidly in recent years. To offset the high initial cost, however, it is essential to maximize the use of solar PV technology [19]. This drives the development of high-efficiency, rapid-switching optimum power point tracking (OPPT) methods [20]. With the growing popularity of PV systems in major cities, it is becoming more challenging to find locations where partial shading conditions (PSC) do not occur for PV panel installations. Because of obstacles like buildings, towers, and trees, the solar irradiation received by PV modules is not evenly distributed [21]. This causes the power-voltage (P-V) curve to have multiple power peaks. The peaks in this curve are referred to as maximum power points (local optimum power point, or LOPP), and the peak with the highest power is referred to as the global optimum power point (GOPP) [22].

It has been found that conventional OPPT algorithms like perturbation and observation (P&O) and incremental conductance are unable to identify the distinction between local and global maximum points. Because of this, conventional approaches to OPP detection fail when partial shading is present [23]. Nonetheless, several studies utilizing OPPT strategies based on computational intelligence algorithms, such as fuzzy logic, evolutionary algorithms, particle swarm optimization, the shuffled frog hopping algorithm, and others, have been implemented to address this difficulty of the conventional techniques [24]. Particle swarm optimization (PSO) is one such technique that is both computationally simple and easy to implement; the major drawbacks of PSO are its lengthy tracking time and its wide search space [25].

In this paper, a SWHPS system consisting of a fuzzy logic controller-based adaptive HCS strategy is used as the OPPT technique, and it is compared to another OPPT strategy with better results, such as the OT control strategy. In order to attain optimal control of rotational speed response, simulation studies were carried out on a 2 MW DFIG to validate the study for wind systems. In addition, in PV systems, a hybrid approach was proposed, which has the benefit of speeding up the tracking process. The hybrid OPPT strategy that combines the P&O and PSO techniques for solar systems under constant and partial shade, this approach offers faster convergence than traditional PSO and reduced oscillations. More energy can be captured through this method compared to the alternatives.

## 2. SOLAR-WIND HYBRID POWER SYSTEM

A solar combined variable-speed wind energy system (SWHPS) is suggested in this proposed research work in which a DFIG is employed to convert wind energy to electrical energy and then integrated with an SPV system through the DC link of the converters, as illustrated in Figure 1. In SWHPS, the estimated capacity of both the solar and wind energy units is considered to be 2.249 MW. Rotor side converter (RSC) assists the wind energy system in operating at the optimal rotational speed specified by the wind OPPT technique. The grid side converter (GSC) regulates the frequency and voltage of the network.
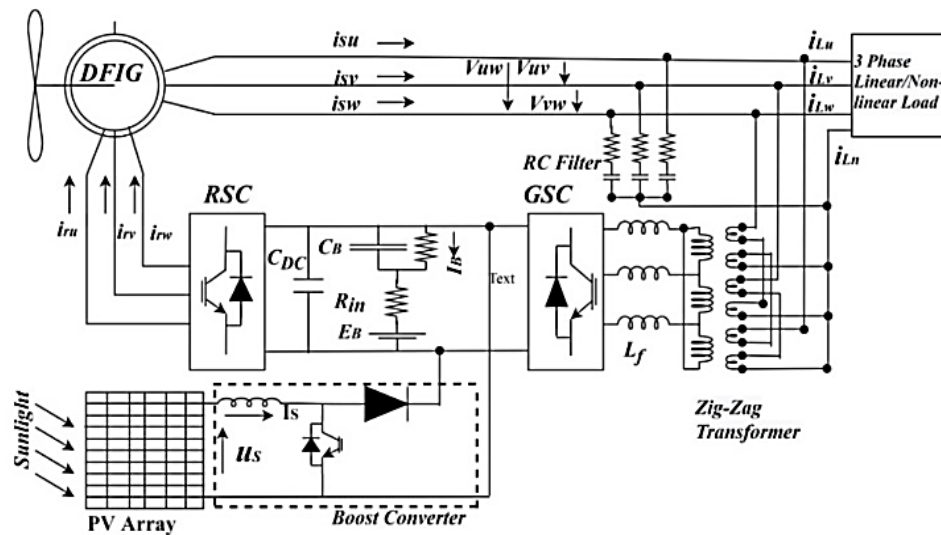


Figure 1. Proposed solar-wind hybrid power system

The obtainable wind power ($P_{obtain}$) can be used to express the correlation between the input of mechanical power and the typical wind velocity of the turbine blades.

$$P_{obtain} = 0.5u^3 A\rho \tag{1}$$

Where $A$ represents the rotor swept area, $\rho$ represents the density of the air, and $u$ represents the wind speed. The expression for the power harnessed by the turbine is denoted as $P_T$, is a quotient of the total power that is obtainable, as represented by (2).

$$P_T = P_{obtain} \times C_P(\lambda \cdot \beta) \tag{2}$$

Where $\lambda$ is the non-dimensional tip speed ratio, $\beta$ is the pitch angle of the blade in radians, and $C_P(\lambda \cdot \beta)$ is the power capture coefficient.

$$\lambda = \frac{\omega_r R}{u} \tag{3}$$

Where R is the blade radius in meters and $\omega_r$ is the rotor speed in radians per second. $T_{aerody}$ represent the aerodynamic torque exerted on the turbine rotor, the resulting power captured can be determined.

$$P_T = T_{aerody}\omega_r \tag{4}$$

The mathematical equation for $T_{aerody}$ can be obtained by integrating (1), (2), and (4) and solving for it.

$$T_{aerody} = \gamma(u, \omega_r)\,C_P(\lambda, \beta) \tag{5}$$

Where, $\gamma = (1/2\omega_r)\,u^3 A\rho$ for $\omega_r > 0$. Using the TSR in (3), one can demonstrate that $T_{aerody}$ is proportional to the $\omega_r^2$. The rotor shaft was mentioned in the motion equation for a connected generator and WT.

$$T_{aerody} - T_E = J\frac{d\omega_r}{dt} + G_D\omega_r \tag{6}$$

Where $J$ is the corresponding total mass of the gearbox, rotor shaft, and blades; $G_D$ is the gearbox's friction coefficient; and $T_E$ is the generator's electrical torque.

## 2.1. dq0-reference frame DFIG model

If the stator and rotor parameters are changed into the rotating frame of reference, the mutual inductances between the stator-rotor exhibit independence with respect to both the speed of the high-speed rotor ( $\omega_r$ ), and position ($\theta_r$). The $dq0$ conversion is utilized to change the $abc$ quantities in the $dq0$ reference frame with an angle disparity between the frames [26]. Applying Kirchhoff's voltage law (KVL) for the stator windings and the Park translation, stator winding differential equations are as (7) and (8).

$$V_{sq} = -R_s i_{sq} + \frac{d\lambda_{sq}}{dt} - \omega\lambda_{sd} \tag{7}$$

$$V_{sd} = -R_s i_{sd} + \frac{d\lambda_{sd}}{dt} - \omega\lambda_{sq} \tag{8}$$

Where $R_s$ represents resistance/phase of the stator winding and $\omega$ represents the frame's angular velocity. These equations are depicted as block diagrams in Figure 2. Similar computational procedures can be applied to the rotor circuits by substituting $(\theta - \theta_r)$ for the term in the $dq0$ conversion for rotor quantities.

$$V_{rq} = R_r i_{srq} + \frac{d\lambda_{rq}}{dt} + (\omega - \omega_r)\lambda_{rd} \tag{9}$$

$$V_{rd} = -R_r i_{rd} + \frac{d\lambda_{rd}}{dt} - (\omega - \omega_r)\lambda_{rq} \tag{10}$$

Additionally, the stator-flux coupling formulae can also be translated to the $dq0$ frame of reference as (11) and (12).

$$\lambda_{sq} = -L_s i_{sq} + L_m i_{rq} \tag{11}$$

$$\lambda_{sd} = -L_s i_{sd} + L_m i_{rd} \tag{12}$$

Where $L_s$ and $L_m$ indicates stator-self and mutual-inductance. Similarly, the rotor flux coupling equations can be transformed to the $dq0$ reference frame as (13) and (14).

$$\lambda_{rq} = L_r i_{rq} - L_m i_{sq} \tag{13}$$

$$\lambda_{rd} = L_r i_{rd} - L_m i_{sd} \tag{14}$$

Where $L_r$ is self-inductance of the rotor. Finally, the derived DFIG electromagnetic torque is given as (15).

$$T_E = 0.75 * P(i_{sq}\lambda_{sd} - i_{sd}\lambda_{sq}) \tag{15}$$

Where $P$ is the pole count. The (7) through (15) are all that are required to design a DFIG in this study. The grid detects the stator voltages, $V_{sd}$ and $V_{sq}$, and the rotor currents, $i_{sd}$ and $i_{sq}$, are regulated by the rotor-side converter; consequently, $\lambda_{sq}$ and $\lambda_{sd}$ are acquired as depicted in Figure 2. Other variables can be determined using mathematical equation, such as $i_{sd}$, $i_{sq}$, from (9) and (10) (ignoring $\frac{d\lambda_{rq}}{dt}$ and $\frac{d\lambda_{rd}}{dt}$) and $T_E$ from (15).

Power converters exhibit significantly quicker dynamics compared to generators and windmills. Consequently, in order to investigate slow dynamic occurrences, it is possible to design the rotor and grid-side converters using their respective controls and 1st-order transfer functions, as depicted in Figure 3. In the RSC, $i_{rd}$ is fixed at zero, and $i_{rq}$ is controlled by the required electrical torque, $T_E^*$. The GSC should estimate both the power and the DC-link voltage. Nevertheless, the power of the GSC can be estimated as (16).

$$P_i = 1.5(i_{iq}V_{iq} - i_{id}V_{id}) \tag{16}$$

Where $V_{id}$ and $V_{iq}$ denote the direct and quadrature inverter voltages, correspondingly, and are derived from $V_{sd}$ and $V_{sq}$, as can be observed. The GSC-links the grid and the stator with a modified low-pass filter represented by an RL circuit. The $dq0$ transformation and KVL equations are used to derive $V_{id}$ and $V_{iq}$, respectively.

$$V_{id} = V_{sd} - R_f i_{id} - L_f \frac{di_{id}}{dt} + L_f \omega i_{iq} \tag{17}$$

$$V_{iq} = V_{sq} - R_f i_{iq} - L_f \frac{di_{iq}}{dt} - L_f \omega i_{id} \tag{18}$$

$V_{sd}$ and $V_{sq}$ are derived from an equivalent set of mathematical equations for the power line, considering the known grid voltage. Utilizing Kirchhoff's current law (KCL) and ignoring the conduction loss of the converters, the voltage on the DC-bus is determined as (19).

$$\frac{0.5}{C}\frac{d(V_{DC}^2)}{dt} = P_r - P_i \tag{19}$$

$C$ represents capacitor on the DC-bus, $P_i$ and $P_r$ represents grid and rotor side converter power. Back-to-back converters have their $i_{rq}$ values determined by the electrical torque they need to generate, whereas rotor-side converters have their $i_{iq}$ values determined by the DC-bus voltage they need to generate their required active power in the GSC. Each of these converter designs is depicted in Figures 3(a) and 3(b).
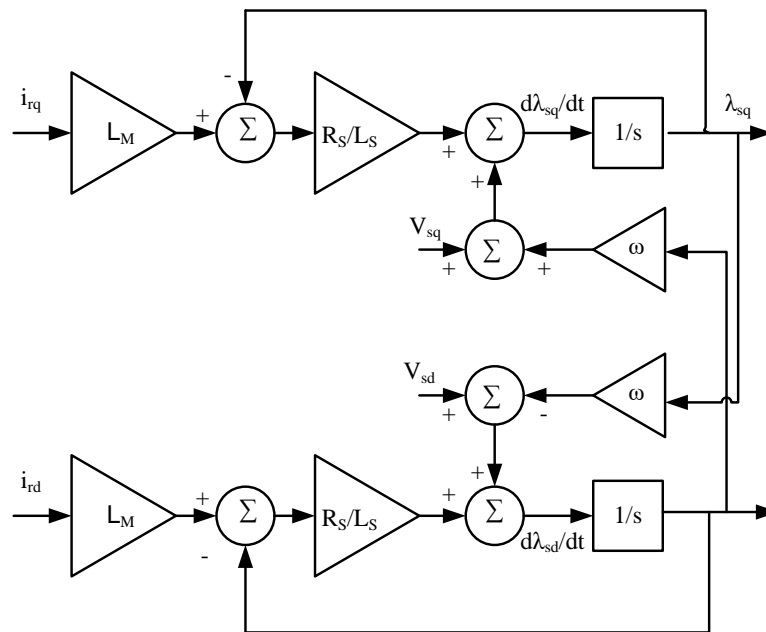


Figure 2. Computations of stator flux, $\lambda_{sd}$ and $\lambda_{sq}$, based on the given input signals $i_{rd}$, $i_{rq}$, $V_{sq}$, and $V_{sd}$
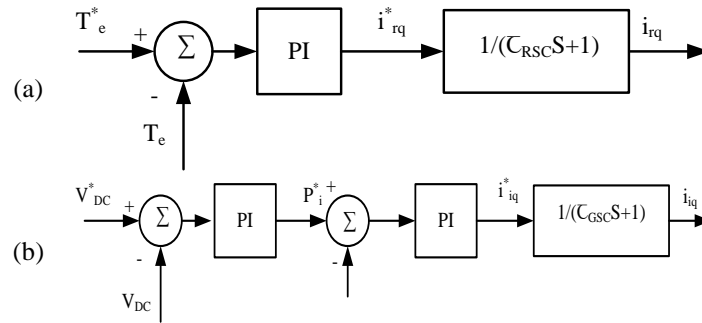
Figure 3. Converter controller: (a) RSC, $i_{rq}$ controlled according to the required $T_e^*$ and (b) GSC, $i_{iq}$ controlled according to the required $V_{DC}^*$

## 3. OPTIMIZATION ALGORITHM FOR SOLAR-WIND HYBRID POWER SYSTEM

This investigation will use the determined speed of rotation as input and the obtained power as output for the system. To determine the appropriate perturbation size, one can rely on fuzzy logic controller (FLC), the variation in speed and mechanical power are used as input parameters ($\partial \omega_M \ and \ \partial P_M$), and the change in reference speed is the output ($\partial \omega_M^*$). Figure 4 depicts fuzzy controller membership functions. Triangular uniform membership functions are a viable option for both input and output, as they offer higher sensitivity, particularly when parameters reach zero [27]. The FLC operates on the basis of perturbing the speed of reference and observing the ensuing variation in power. If there was an increase in output power alongside the most recent speed rise, the search would go in the same direction. Conversely, if increasing the speed results in a decrease in power output, the search direction will be reversed [28], [29].

Table 1 presents the rule table that corresponds to the fuzzy-HCS (FHCS) controller. The FHCS is an effective technique for tracking the optimum power point, particularly when wind conditions are frequently changing. Figure 5 depicts the schematic diagram of the OPPT control. Taking into consideration the power losses in the drivetrain and assuming the converters are lossless, the mechanical power can be calculated using (20).

$$P_{M\_esti} = P_r + P_s + P_{LOSS\_DT} = (1 - g)P_s + P_{LOSS\_DT} \tag{20}$$

$$T_{HSS\_OPT} = 0.5R^5\pi\rho \frac{C_{PMAX}}{\lambda_{OPT}^3} \omega_m^2 = K_{OPT}\omega_m^2 \tag{21}$$

The technique employed depends on torque control, whereby the optimal torque curve is expressed mathematically as (21) and used as a reference torque for the controller that is linked to the WT. The frictional loss in torque is so negligible that it is ignored by our control system as well. Figure 6 depicts a detailed schematic of the OT control. Figure 7 depicts the suggested H-OPPT algorithm's flowchart. The algorithm keeps the operating point at the OPP through P&O until it detects partial shade [30], [31].

In the "OP-track sub-program," the suitable voltage range is selected. This region is scanned by the PSO, which returns the highest Pi value. The importance of tracking future peaks is examined. If the power disparity condition is met, the value of the GOPP is calculated by contrasting each of the recorded OPP power values. If the criterion fails, the similar operation is continued till all peaks are considered. When the "OP-track sub-program" returns, the P&O technique continues to keep the operating point at the OPPT [32], [33].

The SPV system is associated to the back-to-back (BTB) which converter the DC-link. Since the DC power produced can be supplied into the grid, no additional inverter is required. MATLAB/Simulink are used to simulate a stand-alone SPV system with various OPPT techniques. To select the best OPPT method for a stand-alone SPV scheme, Simulink modeling of the scheme is developed and connected to the boost converter.

Table 1. Presents the rule table that corresponds to the fuzzy-HCS (FHCS) controller

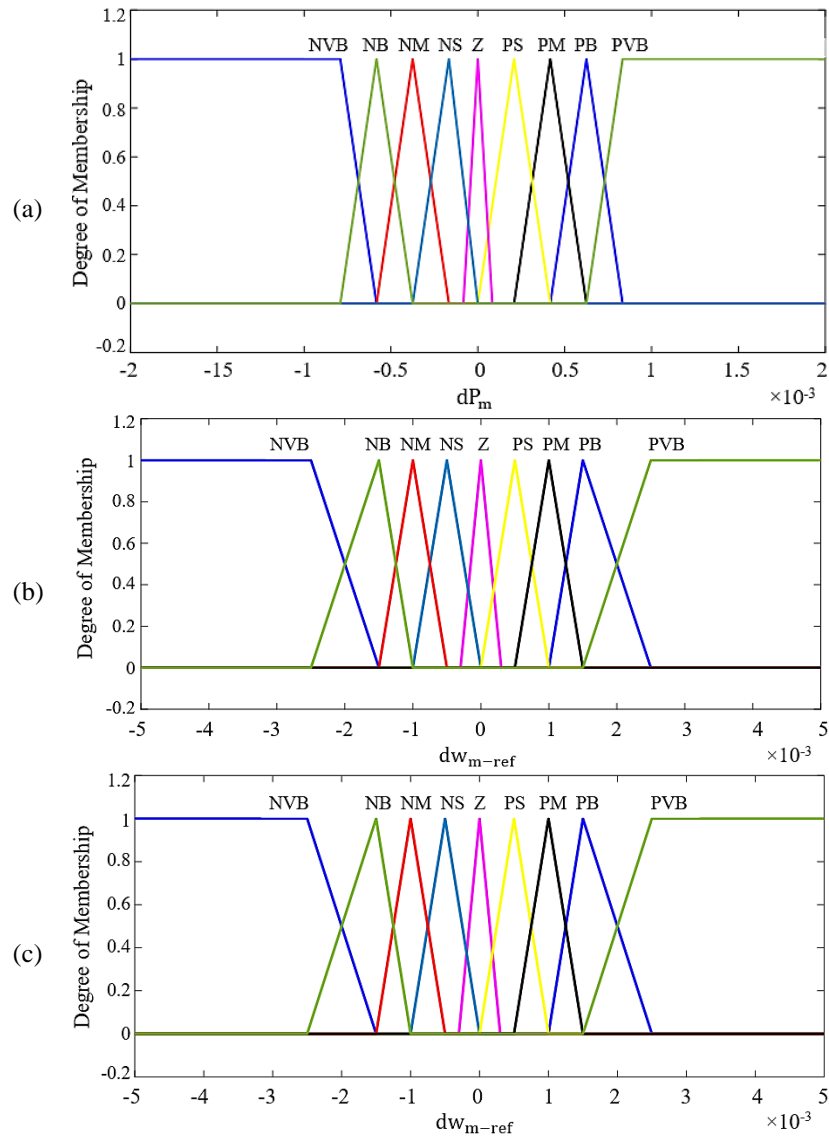| $\partial \omega_m$ | $\partial P_m$ | | | | | | | | |
|---|---|---|---|---|---|---|---|---|---|
| | NVB | NB | NM | NS | Z | PS | PM | PB | PVB |
| N | PVB | PB | PM | PS | Z | NS | NM | NB | NVB |
| Z | NB | NM | NS | NS | Z | PS | PM | PM | PB |
| P | NVB | NB | NM | NS | Z | PM | PM | PB | PVB |

Figure 4. Depicts fuzzy controller membership functions: (a) input $\omega_M$, (b) input $\partial P_M$, and (c) output membership

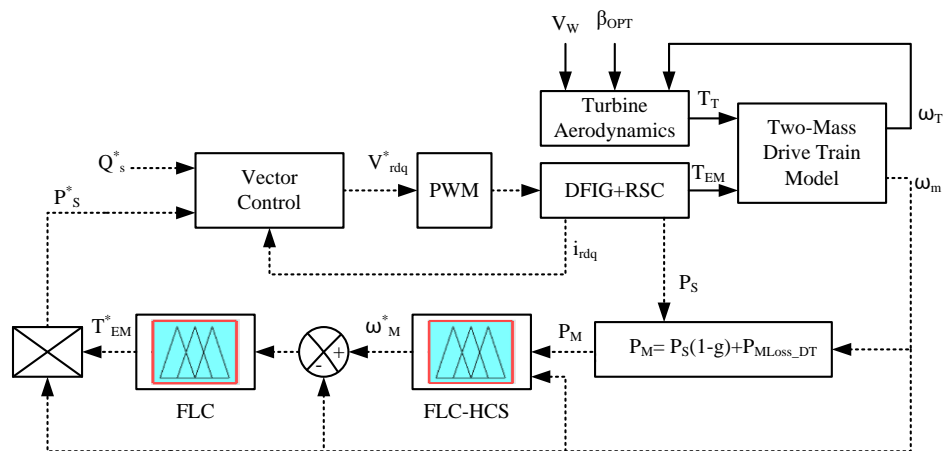

Figure 5. Depicts a detailed schematic of the OPPT control
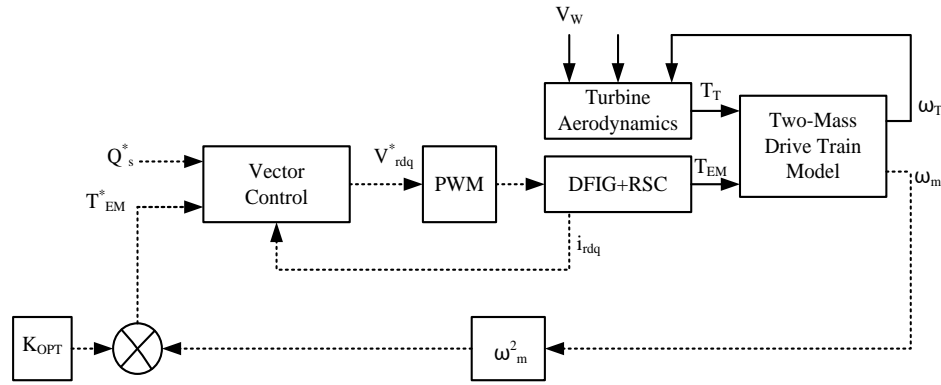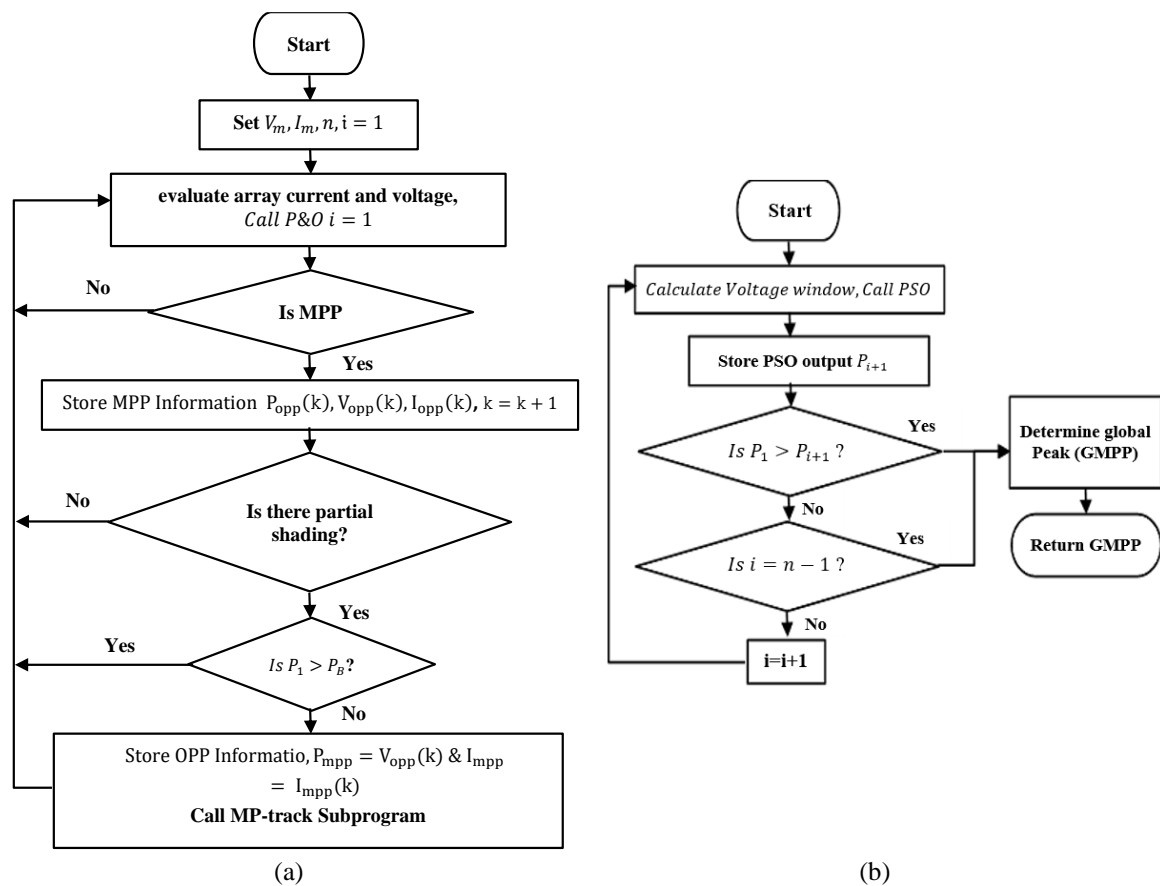
Figure 6. Depicts a detailed schematic of the OT control



|        (a)        |        (b)        |

Figure 7. Flowcharts for the suggested hybrid PSO-P&O MPPT method: (a) main-program
and (b) OP-track sub-program

## 4. RESULTS AND DISCUSSION

The suggested SWHPS design is modeled utilizing the MATLAB/Simulink platform, including the PV, WT, BTB converter, DFIG device, transformer, and grid filter. The DFIG device is linked to the grid through the stator. The rotor is linked to the grid through a BTB converter and transformer.

### 4.1. Validation of Solar PV OPPT for SWHPS

The module utilized for simulation is an array type: Trina Solar TSM-250PA05.38, 10 series modules, 100 parallel strings. Table 2 contains the detailed specifications for the solar module. The hybrid PSO-P&O, PSO, and P&O OPPT approaches have been applied to this system, and the efficiencies of all three have been compared.

Table 3 shows an overview of the evaluation results for the MPPT methods performed in the first and second cases. For the first case, which simulates constant shading conditions, it is evident that all the algorithms effectively track the GOPP. This demonstrates that the HPOPSO technique presented in this work is capable of extracting more power under a constant regime with no changes to environmental circumstances.

In the second case, a time interval in which a variation in shading circumstances occurs is evaluated. It begins with uniform shade conditions, with solar irradiance of $1000 \frac{W}{m^2}$, and after some time, the solar irradiance reduces to $800 \frac{W}{m^2}$, $600 \frac{W}{m^2}$, $400 \frac{W}{m^2}$, and $200 \frac{W}{m^2}$ in PV modules at $t = 0\ s$, $t = 2\ s$, $t = 3\ s$, and $t = 4\ s$, indicating the transition from uniform to partial shading. Comparing the suggested method to traditional PSO and P&O, it is evident that the suggested method has a faster convergence rate, thereby lowering the tracking time. It has the benefit of steadiness under the permanent regime, which translates to a greater power output as shown in Figures 8 and 9.

Table 2. Solar module parameters for simulation of SPV, OPPT, and SWHPS

| Parameter | Value | Parameter | Value |
|---|---|---|---|
| Maximum power ($P_{MAX}$) | 249.85 W | Open circuit voltage ($V_{OC}$) | 37.6 V |
| Maximum current ($I_{MAX}$) | 8.06 A | Series modules | 10 |
| Short circuit current ($I_{SC}$) | 8.55 A | Parallel strings | 100 |
| Maximum voltage ($V_{MAX}$) | 31 V | | |

Table 3. The effectiveness of the OPPT techniques in the different irradiation conditions

| Parameter | | Proposed HPOPSO | P&O | PSO |
|---|---|---|---|---|
| First case-constant shading condition | Maximum power (W) | $2.472 \times 10^5$ | $2.370 \times 10^5$ | $1.848 \times 10^5$ |
| | Mean power (W) | $2.055 \times 10^5$ | $1.889 \times 10^5$ | $1.699 \times 10^5$ |
| | Maximum voltage (V) | 2723 | 2722 | 2354 |
| | Mean voltage (V) | 2419 | 2370 | 2235 |
| Second case-partial shading condition | Maximum power (W) | $2.315 \times 10^5$ | $2.101 \times 10^5$ | $2.267 \times 10^5$ |
| | Mean power (W) | $9.926 \times 10^4$ | $9.643 \times 10^4$ | $9.142 \times 10^4$ |
| | Maximum voltage (V) | 2635 | 2608 | 2317 |
| | Mean voltage (V) | 1627 | 1587 | 1617 |
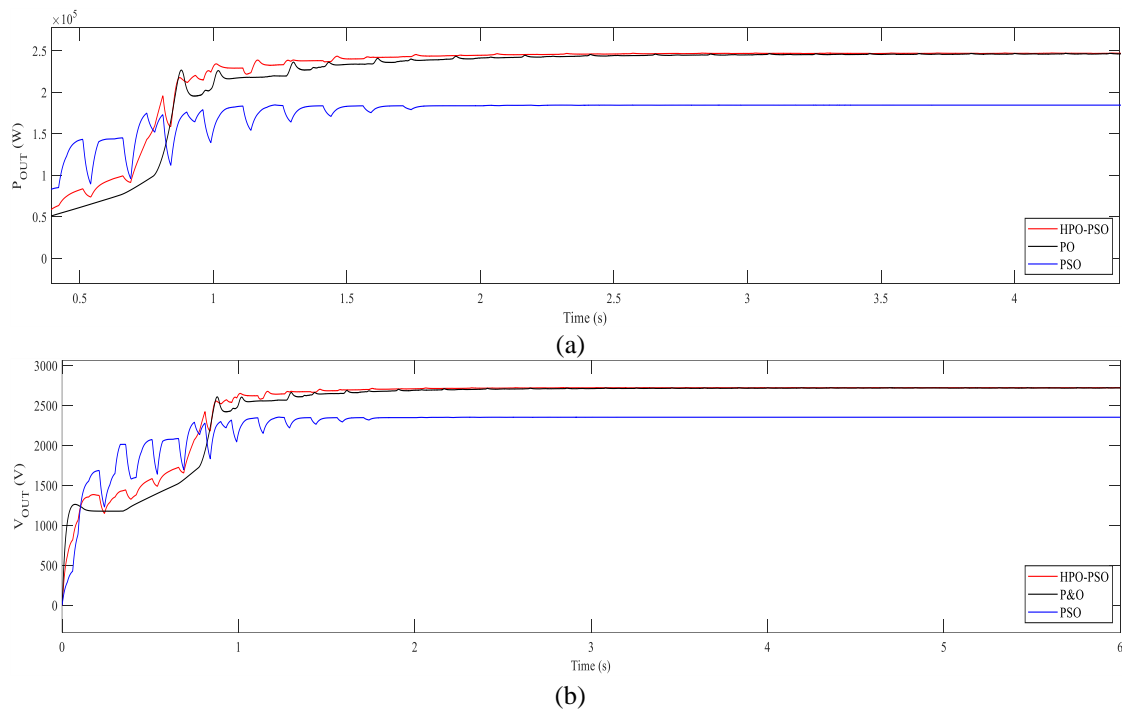


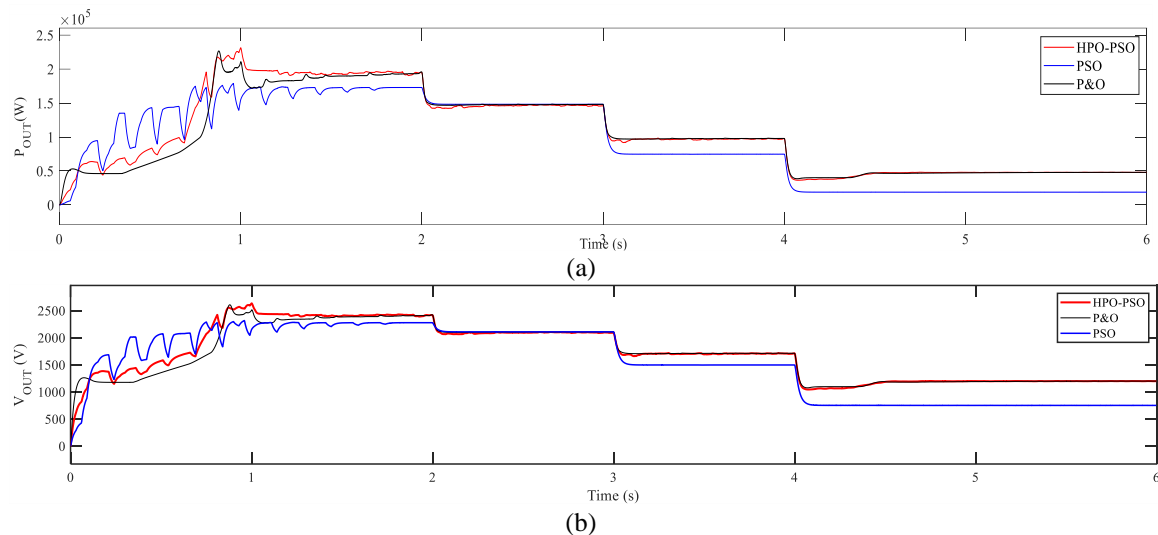Figure 8. Case 1-hybrid PSO-P&O, PSO: (a) output power vs. time and (b) output voltage vs. time

Figure 9. Case 2-hybrid PSO-P&O, PSO: (a) output power vs. time and (b) output voltage vs. time

## 4.2. Validation of DFIG-WT MPPT

A study was conducted on a 2 MW DFIG system with the suggested adaptive fuzzy-HCS (FHCS) controller. The DFIG specifications are listed in Table 4. The aim of the simulation is to implement a stepped-wind speed in an abrupt manner with the purpose of emulating potent wind turbulence. The suggested FHCS technique should provide the optimum rotating speed for the system and compete with the OT control technique with regard to effectiveness and response speed.

Figure 10(a) (see Appendix) displays a wind speed that includes a range of variable speeds, spanning from the cut-in to the rated wind speeds. Figure 10(b) (see Appendix) displays the change in rotational speed and its corresponding conceptual optimum speed, which vary in accordance with variations in wind speed. The FHCS technique seems to be faster and more stable, even when the wind speed changes, compared to the OT control. Figure 10(c) (see Appendix) shows the DFIG's output power, the WT's rated power, and the theoretical optimum mechanical power. The FHCS control technique seems more stable, while the OT has problems with oscillations. Regarding efficiency, both OPPT techniques yield almost identical average amounts of power, particularly at medium wind speeds.

Figure 10(d) (see Appendix) displays the electrical torque and the associated mechanical torque for each OPPT technique. The dynamics of both of these torques highlight the distinction between the two OPPT techniques. The OT control technique is more stable and slower as it employs the calculated optimum torque and utilizes the slow dynamic of the speed of rotation, this dynamic is dependent on the WT's inertia. Whereas, the FHCS technique employs a closed-loop speed control system that adjusts the speed of reference based on the distance between the optimum and actual operational points. The huge fluctuations observed in the FHCS technique provide evidence of its superior dynamic response. Figures 10(e) and 10(f) (see Appendix) display the rotor and stator currents generated through the OT and FHCS power optimization techniques; they vary based on the magnitude of the output power, while the frequency of the rotor current varies based on the rotating speed, whereas the frequency of the stator currents is kept at the same level as the grid frequency. Furthermore, it is evident that the FHCS control technique is greater stable compared to the OT technique.

Figure 10(g) (see Appendix) displays the $C_P$ response. In terms of speed, both techniques appear to be nearly equal. However, the FHCS technique outperforms in sustaining the optimal value of $C_P$ regardless of wind speed changes. However, the OT faces an issue with the step-size seeking process while in steady-state operation. The time required for this procedure depends on the mechanical features of the WT. Nevertheless, the variance between them, which is 0.51–0.49, can be considered acceptable.) displays the TSR attributes, which accomplish the optimum level and maintain it across both OPPT techniques. Figure 10(h) (see Appendix) illustrates the pitch angle changes based on the system's operating point, ranging from 0 to 3.3 s. During this time, the pitch orientation system operates to restrict the power and speed to the rated points. However, after this period, the pitch orientation system is disengaged to enable the OPPT system to function without any restrictions. According to simulation findings and evaluation, the FHCS technique was found to be the most stable and effective because it keeps looking for the best operating point without needing to know any information regarding the wind speed or WT characteristics. The OT technique is fast but less effective at maintaining steady state, but its dependence on WT characteristics rendered it inflexible.

Table 4. DFIG parameters for the simulation of WT-MPPT and SWHPS

| Parameters | Value |
|---|---|
| Rated power ($P_{RATED}$) | 2.0 $MW$ |
| Rated torque($T_{RATED}$) | 12734 $Nm$ |
| Stator current ($I_S$) | 1.980 $kA$ |
| Working frequency | 50 $Hz$ |
| Switching frequency | 4 $KHz$ |
| Rated rotor voltage | 2.072 $kV$ |
| DC bus voltage | 1.154 $kV$ |
| Stator voltage ($V_{STAOR}$) | 0.692 $kV$ |
| No of pole pairs | 2 |
| Speed of the rotor shaft | 1500 $rpm$ |
| $L_M$ | 2.6 $mH$ |
| $R_R$ | 2.90 $m\Omega$ |
| $R_S$ | 2.8 $m\Omega$ |
| $\Sigma$ | 0.088 $mH$ |

## 5.    CONCLUSION

This study examines and discusses an adaptive OPPT algorithm for DFIG-equipped WT systems and solar PV systems. The result of simulations on a standalone SPV scheme using hybrid PSO-P&O evidently presented the technique as more efficient than PSO and P&O OPPT techniques. The suggested hybrid algorithm was able to successfully follow OPP in both constant and varying shade scenarios, with tracking times that were 50% faster than those achieved using the traditional PSO and P&O techniques. Also, the proposed technology can increase the amount of energy made by the PV system by 0.3%. Also, this research examined a simulation and made a comparison between the suggested technique and the traditional OT control technique with respect to efficiency and response time. Simulations showed that the OT and fuzzy-HCS control methods were almost as accurate as each other. The OT technique is also quick response, flexible, and efficient, but it can be hard to figure out what the best step size is, which can lead to more fluctuating results. Nevertheless, its inflexibility was attributed to its reliance on the specific characteristics of wind turbines. The fuzzy-HCS methodology achieved the highest mean Cp value and exhibited superior capacity for maintaining this maximum value, even when subjected to variations in wind velocity, as compared to the OT approach. By choosing the appropriate adaptive step-size techniques, it is possible to enhance performance and address the issues in the suggested technique.

## FUNDING INFORMATION

## AUTHOR CONTRIBUTIONS STATEMENT

This journal uses the Contributor Roles Taxonomy (CRediT) to recognize individual author contributions, reduce authorship disputes, and facilitate collaboration.

| Name of Author | C | M | So | Va | Fo | I | R | D | O | E | Vi | Su | P | Fu |
|---|---|---|---|---|---|---|---|---|---|---|---|---|---|---|
| G. B. Arjun Kumar | ✓ | ✓ | ✓ | ✓ | ✓ | ✓ | ✓ | ✓ | ✓ | ✓ | | ✓ | ✓ | |
| M. Balamurugan | ✓ | ✓ | ✓ | | ✓ | ✓ | | ✓ | ✓ | ✓ | ✓ | | | |
| K. N. Sunil Kumar | ✓ | | ✓ | ✓ | | ✓ | ✓ | | ✓ | ✓ | ✓ | | ✓ | |
| Ravi Gatti | ✓ | | | ✓ | | | ✓ | | ✓ | ✓ | ✓ | | ✓ | |

| | | | | | | |
|---|---|---|---|---|---|---|
| C : **C**onceptualization | | I : **I**nvestigation | | Vi : **Vi**sualization | |
| M : **M**ethodology | | R : **R**esources | | Su : **Su**pervision | |
| So : **So**ftware | | D : **D**ata Curation | | P : **P**roject administration | |
| Va : **Va**lidation | | O : Writing - **O**riginal Draft | | Fu : **Fu**nding acquisition | |
| Fo : **Fo**rmal analysis | | E : Writing - Review & **E**diting | | | |

## CONFLICT OF INTEREST STATEMENT

The authors declare that the research was conducted in the absence of any commercial or financial relationships that could be construed as a potential conflict of interest.

## DATA AVAILABILITY

The data that support the findings of this study are available from the corresponding author, [GBAK], upon reasonable request.

## REFERENCES

[1]     D. A. Ciupăgeanu, G. Lăzăroiu, and L. Barelli, "Wind energy integration: Variability analysis and power system impact assessment," *Energy*, vol. 185, pp. 1183–1196, 2019, doi: 10.1016/j.energy.2019.07.136.

[2]     M. Balamurugan, K. Narayanan, N. Raghu, G. B. A. Kumar, and V. N. Trupti, "Role of artificial intelligence in smart grid – a mini review," *Frontiers in Artificial Intelligence*, vol. 8, p. 1551661, 2025, doi: 10.3389/frai.2025.1551661.

[3]     D. A. Ciupageanu, L. Barelli, and G. Lazaroiu, "Real-time stochastic power management strategies in hybrid renewable energy systems: A review of key applications and perspectives," *Electric Power Systems Research*, vol. 187, 2020, doi: 10.1016/j.epsr.2020.106497.

[4]     A. Mahesh and K. S. Sandhu, "Hybrid wind/photovoltaic energy system developments: Critical review and findings," *Renewable and Sustainable Energy Reviews*, vol. 52, pp. 1135–1147, 2015, doi: 10.1016/j.rser.2015.08.008.

[5]     A. Kumar, Shivashankar, and B. S. Ram, "Efficient solar integrated doubly fed induction generator for wind energy harnessing," *Recent Advances in Electrical & Electronic Engineering (Formerly Recent Patents on Electrical & Electronic Engineering)*, vol. 13, no. 5, pp. 723–735, 2019, doi: 10.2174/2352096512666191019094707.

[6]     G. B. A. Kumar and Shivashankar, "Optimal power point tracking of solar and wind energy in a hybrid wind solar energy system," *International Journal of Energy and Environmental Engineering*, vol. 13, no. 1, pp. 77–103, 2022, doi: 10.1007/s40095-021-00399-9.

[7]     A. M. Hemeida *et al.*, "Optimum design of hybrid wind/PV energy system for remote area," *Ain Shams Engineering Journal*, vol. 11, no. 1, pp. 11–23, 2020, doi: 10.1016/j.asej.2019.08.005.

[8]     J. F. Manwell, "Hybrid Energy Systems," in *Encyclopedia of Energy*, 2004, pp. 215–229, doi: 10.1016/B0-12-176480-X/00360-0.

[9]     B. M. K. Kumar, S. N. Rao, and M. S. Indira, "Analysis of grid-connected reduced switch MLI with high-gain interleaved boost converter and hybrid MPPT for solar PV," *International Journal of Energy and Environmental Engineering*, vol. 13, no. 4, pp. 1287–1307, 2022, doi: 10.1007/s40095-022-00479-4.

[10]    A. Goswami, P. Sadhu, and P. K. Sadhu, "Development of a grid connected solar-wind hybrid system with reduction in levelized tariff for a remote island in India," *Journal of Solar Energy Engineering, Transactions of the ASME*, vol. 142, no. 4, 2020, doi: 10.1115/1.4046147.

[11]    MNRE, "Ministry of new and renewable energy," [Online]. Available: https://mnre.gov.in/img/documents/uploads/ 2775b59919174bb 7aeb00bb1d5cd269c.pdf. Accessed: Jan. 5, 2021.

[12]    G. S. Kaloi, J. Wang, and M. H. Baloch, "Active and reactive power control of the doubly fed induction generator based on wind energy conversion system," *Energy Reports*, vol. 2, pp. 194–200, 2016, doi: 10.1016/j.egyr.2016.08.001.

[13]    S. Rehman, "Hybrid power systems – sizes, efficiencies, and economics," *Energy Exploration and Exploitation*, vol. 39, no. 1, pp. 3–43, 2021, doi: 10.1177/0144598720965022.

[14]    B. Bhandari, S. R. Poudel, K. T. Lee, and S. H. Ahn, "Mathematical modeling of hybrid renewable energy system: A review on small hydro-solar-wind power generation," *International Journal of Precision Engineering and Manufacturing - Green Technology*, vol. 1, no. 2, pp. 157–173, 2014, doi: 10.1007/s40684-014-0021-4.

[15]    A. Acakpovi, P. Adjei, N. Nwulu, and N. Y. Asabere, "Optimal hybrid renewable energy system: a comparative study of wind/hydrogen/fuel-cell and wind/battery storage," *Journal of Electrical and Computer Engineering*, vol. 2020, 2020, doi: 10.1155/2020/1756503.

[16]    R. Zhu, A. Zhao, G. Wang, X. Xia, and Y. Yang, "An energy storage performance improvement model for grid-connected wind-solar hybrid energy storage system," *Computational Intelligence and Neuroscience*, vol. 2020, pp. 1–10, Aug. 2020, doi: 10.1155/2020/8887227.

[17]    M. K. Bourdoulis and A. T. Alexandridis, "PI control design and passivity/stability analysis for DFIG wind systems under vector control constraints," in *Proceedings of the IASTED International Conference on Control and Applications, CA 2012*, 2012, pp. 127–134, doi: 10.2316/P.2012.781-035.

[18]    S. Karad and R. Thakur, "Recent trends of control strategies for doubly fed induction generator based wind turbine systems: a comparative review," *Archives of Computational Methods in Engineering*, vol. 28, no. 1, pp. 15–29, 2021, doi: 10.1007/s11831-019-09367-3.

[19]    M. A. Soliman, H. M. Hasanien, and A. Alkuhayli, "Marine predators algorithm for parameters identification of triple-diode photovoltaic models," *IEEE Access*, vol. 8, pp. 155832–155842, 2020, doi: 10.1109/ACCESS.2020.3019244.

[20]    A. O. Baba, G. Liu, and X. Chen, "Classification and evaluation review of maximum power point tracking methods," *Sustainable Futures*, vol. 2, 2020, doi: 10.1016/j.sftr.2020.100020.

[21]    B. Pakkiraiah and G. D. Sukumar, "Research survey on various MPPT performance issues to improve the solar PV system efficiency," *Journal of Solar Energy*, vol. 2016, pp. 1–20, 2016, doi: 10.1155/2016/8012432.

[22]    M. Kamran, M. Mudassar, M. R. Fazal, M. U. Asghar, M. Bilal, and R. Asghar, "Implementation of improved Perturb & Observe MPPT technique with confined search space for standalone photovoltaic system," *Journal of King Saud University - Engineering Sciences*, vol. 32, no. 7, pp. 432–441, 2020, doi: 10.1016/j.jksues.2018.04.006.

[23]    H. H. H. Mousa, A. R. Youssef, and E. E. M. Mohamed, "Hybrid and adaptive sectors P&O MPPT algorithm based wind generation system," *Renewable Energy*, vol. 145, pp. 1412–1429, 2020, doi: 10.1016/j.renene.2019.06.078.

[24]    I. Yazici and E. K. Yaylaci, "Improving Efficiency of the Tip Speed Ratio-MPPT Method for Wind Energy Systems by Using an Integral Sliding Mode Voltage Regulator," *Journal of Energy Resources Technology, Transactions of the ASME*, vol. 140, no. 5, 2018, doi: 10.1115/1.4038485.

[25]    D. Song, J. Yang, M. Su, A. Liu, Y. Liu, and Y. H. Joo, "A comparison study between two MPPT control methods for a large variable-speed wind turbine under different wind speed characteristics," *Energies*, vol. 10, no. 5, 2017, doi: 10.3390/en10050613.

[26]    J. Lebron, L. Castillo, and C. Meneveau, "Experimental study of the kinetic energy budget in a wind turbine streamtube," *Journal of Turbulence*, vol. 13, pp. 1–22, 2012, doi: 10.1080/14685248.2012.705005.

[27]    M. Lara, J. Garrido, M. L. Ruz, and F. Vázquez, "Adaptive pitch controller of a large-scale wind turbine using multi-objective optimization," *Applied Sciences (Switzerland)*, vol. 11, no. 6, 2021, doi: 10.3390/app11062844.

[28]    D. W. Novotny and T. A. Lipo, "Vector Control and dynamics of AC drives," *Vector Control and Dynamics of AC Drives*, 1996, doi: 10.1093/oso/9780198564393.001.0001.

[29]    M. N. Uddin and I. K. Amin, "Adaptive Step size based hill-climb search algorithm for MPPT control of DFIG-WECS with reduced power fluctuation and improved tracking performance," *Electric Power Components and Systems*, vol. 46, no. 19–20, pp. 2203–2214, 2018, doi: 10.1080/15325008.2018.1533603.

[30] S. Chtita *et al.*, "A novel hybrid GWO–PSO-based maximum power point tracking for photovoltaic systems operating under partial shading conditions," *Scientific Reports*, vol. 12, no. 1, 2022, doi: 10.1038/s41598-022-14733-6.

[31] J. P. Ram, D. S. Pillai, N. Rajasekar, and S. M. Strachan, "Detection and identification of global maximum power point operation in solar PV applications using a hybrid ELPSO-PO tracking technique," *IEEE Journal of Emerging and Selected Topics in Power Electronics*, vol. 8, no. 2, pp. 1361–1374, 2020, doi: 10.1109/JESTPE.2019.2900999.

[32] T. N. Olayiwola and S. J. Choi, "Superellipse model: An accurate and easy-to-fit empirical model for photovoltaic panels," *Solar Energy*, vol. 262, 2023, doi: 10.1016/j.solener.2023.05.026.

[33] T. N. Olayiwola, S. H. Hyun, and S. J. Choi, "Photovoltaic modeling: A comprehensive analysis of the I–V characteristic curve," *Sustainability (Switzerland)*, vol. 16, no. 1, 2024, doi: 10.3390/su16010432.

## APPENDIX
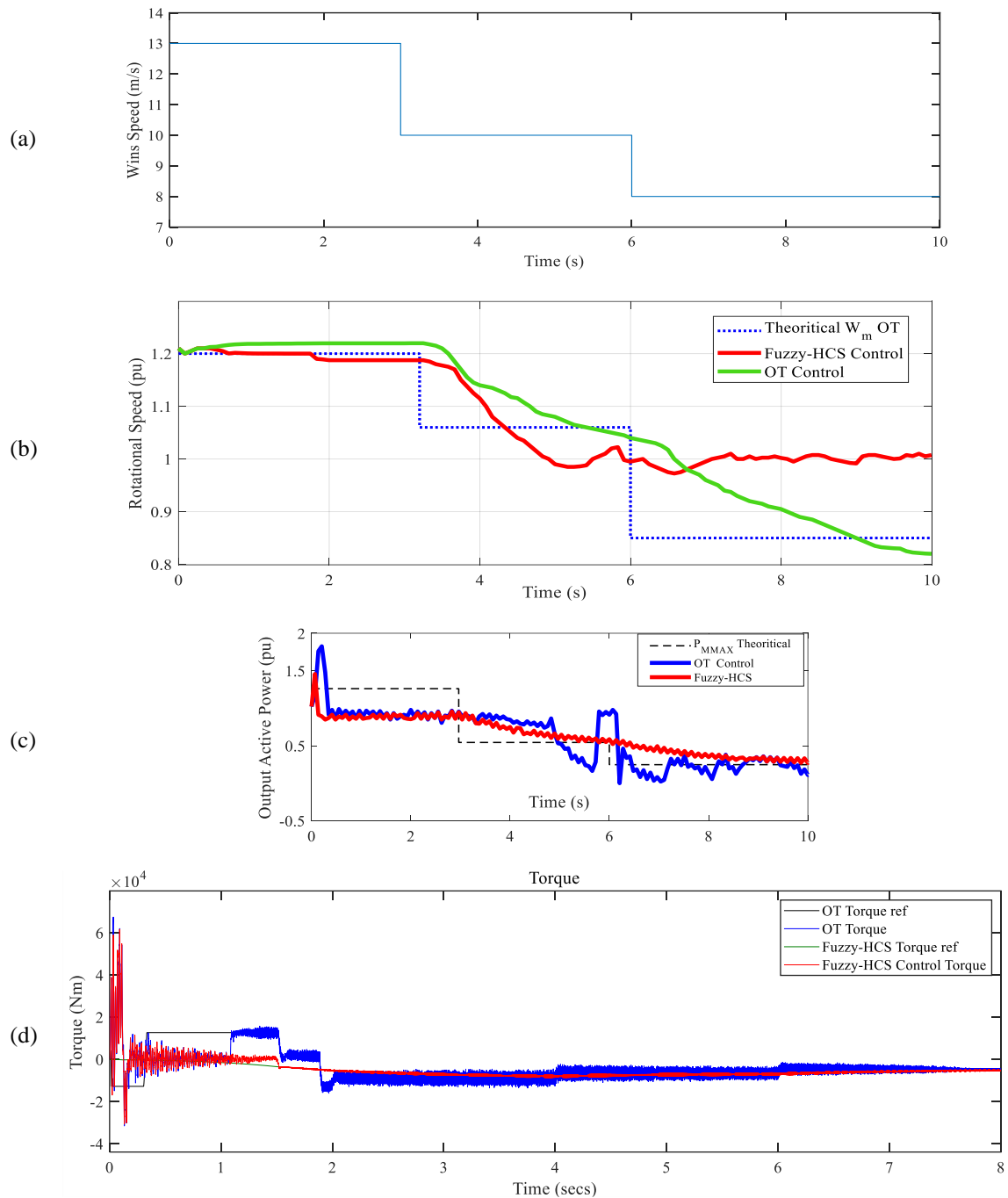


Figure 10. Shows the dynamic responses of the FHSC technique in different speed modes: (a) wind speed, (b) rotational speed, (c) output power, and (d) torque
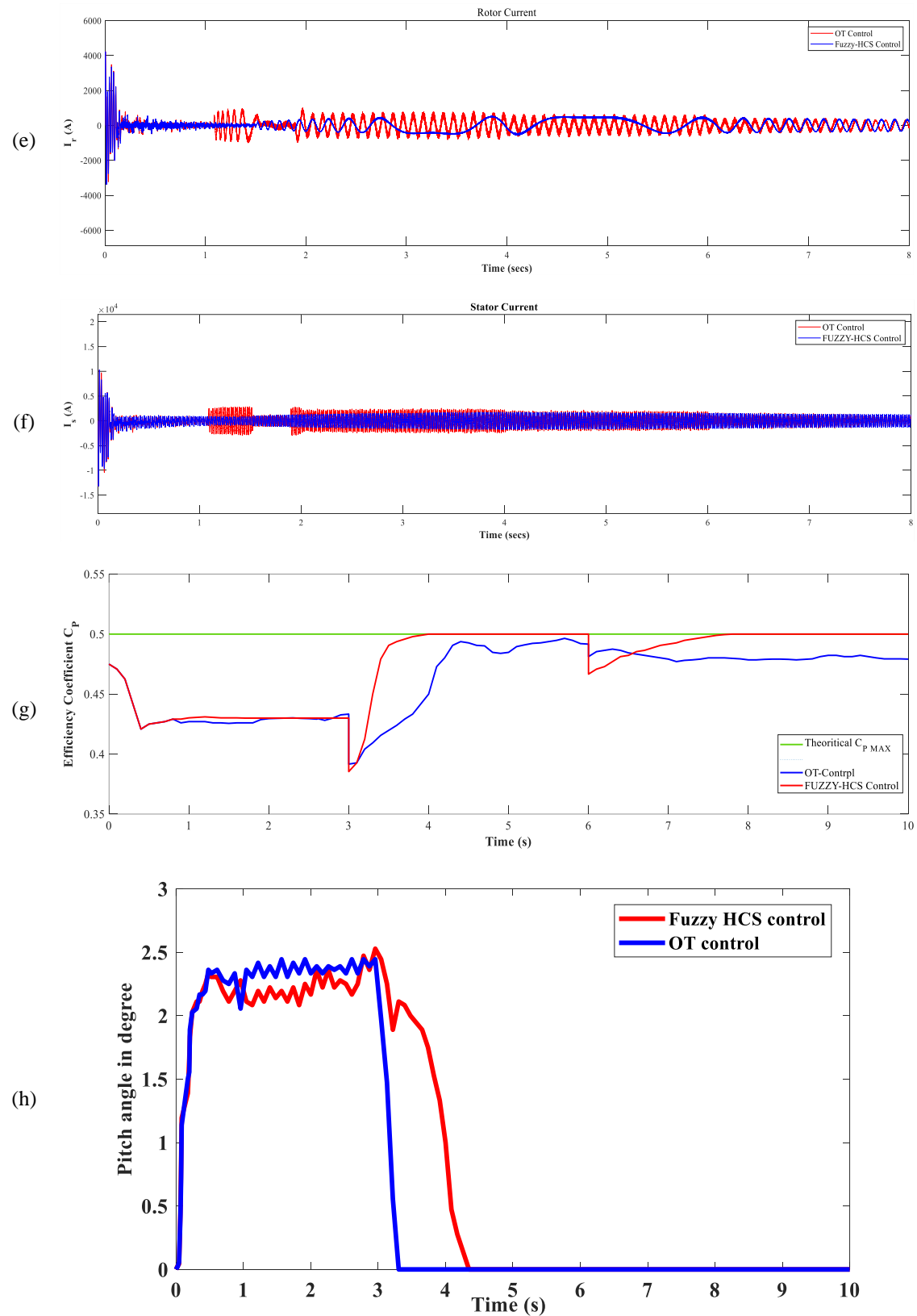
Figure 10. Shows the dynamic responses of the FHSC technique in different speed modes:
(e) rotor current, (f) stator current, (g) efficiency coefficient, and (h) pitch angle (continued)

## BIOGRAPHIES OF AUTHORS

**Dr. G. B. Arjun Kumar** ⓘ 🔢 SC ⬡ has a career spanning over eleven years in the field of industrial and engineering education. Pursued Ph.D. from Visvesvaraya Technological University, Belagavi in the domain of Renewable Energy Resources during 2017-202. Six patents and published more than 30 technical papers related to the domain wind energy, solar energy, hybrid energy, and power electronics in the reputed international journals and international/national conferences. Performed as a reviewer for journals. Currently working as an assistant professor in the Department of Electrical and Electronics Engineering, Dayananda Sagar College of Engineering, Bangalore. He can be contacted at email: arjun-eee@dayanandasagar.edu.

**Dr. M. Balamurugan** ⓘ 🔢 SC ⬡ is currently working as assistant professor in Department of EEE, Dayananda Sagar College of Engineering, Bangalore. He has also awarded as Best Researcher in the year 2016 by VIT University. His research interests are cascaded multilevel inverter and power electronics application in renewable energy systems. He has published several international papers in journals, book chapters, and conferences of high repute. He can be contacted at email: balamurugan-eee@dayanandasagar.edu.

**Dr. K. N. Sunil Kumar** ⓘ 🔢 SC ⬡ has a career spanning over twelve years in the field of industrial and engineering education. One patent and published more than 24 technical papers related to the domain wireless communication, biomedical signal processing, IoT, and VLSI domain in reputed international journals and international/national conferences. Currently working as professor in the Department of ISE, Sri Venkateshwara College of Engineering, Bangalore. He can be contacted at email: sunilkumarkn26@gmail.com.

**Dr. Ravi Gatti** ⓘ 🔢 SC ⬡ has a career spanning over nine years in the field of industrial and engineering education. He is the author of the several articles published in international/national journals and conferences. Performed as a reviewer for journals including IET on Power Electronics and IEEE Access; and for many IEEE international conferences. His current interest includes wireless networks, scheduling algorithms in LTE-A system, and RRM process. He can be contacted at email: ravigatti-ece@dsatm.edu.in.